How to cite: *Angew. Chem. Int. Ed.* **2025**, e202509589
doi.org/10.1002/anie.202509589

**Direct X-ray Detectors** **Hot Paper**

# Solution-Processed Amorphous Zero-Dimensional Organic Metal Halide Hybrid Films for Direct X-Ray Detectors

*Oluwadara J Olasupo, Abiodun M. Adewolu, Mohammad Khizr, Tarannuma F. Manny, He Liu, Tunde B. Shonde, Md S. Islam, Sahel Moslemi, Ethan Kim, J.S. Raaj V Winfred, Thilina N.D.D. Gamaralalage, Yan-Yan Hu, Ranjan Das, and Biwu Ma**

**Abstract:** Zero-dimensional (0D) organic metal halide hybrids (OMHHs) are emerging materials with significant potential for optoelectronic applications, including direct X-ray detectors. While 0D OMHH single crystals exhibit excellent X-ray detection properties, their scalability remains a significant challenge due to the time-intensive growth process and difficulty in producing large single crystals exceeding a few centimeters. This limitation hinders their practicality for large-area detector applications. Here, we report for the first time the development of amorphous 0D OMHH films via solution processing for efficient direct X-ray detection. By reacting a non-crystalline organic halide, triphenyl(9-phenyl-9H-carbazol-3-yl)phosphonium bromide (TPPCarzBr), with zinc bromide ($ZnBr_2$), we have successfully produced amorphous 0D $(TPPCarz)_2ZnBr_4$ films with controlled thickness via facile solution processing. The organic cations ($TPPCarz^+$) feature a lower bandgap than the $ZnBr_4^{2-}$ anions, enabling efficient molecular sensitization, where $ZnBr_4^{2-}$ anions serve as X-ray absorbers and $TPPCarz^+$ cations as charge transporters. Direct X-ray detectors based on 0D $(TPPCarz)_2ZnBr_4$ films demonstrate outstanding performance, achieving a stable X-ray detection sensitivity of 2,165 $\mu C\ Gy_{air}^{-1} cm^{-2}$ at 20 V $mm^{-1}$ and a detection limit of 6.01 $nGy_{air}\ s^{-1}$. The amorphous nature of these films enhances their processability, allowing for fabrication in various sizes and shapes, and making them highly adaptable for scalable detector applications.

## *Introduction*

Direct X-ray detectors are devices based on semiconductors that convert X-ray photons directly into electrical charges.[1] Upon processing these charges into quantifiable electronic signals, direct X-ray detectors find various applications in photon-counting computed tomography (PCCT) for disease detection, radiography, real-time dosimetry for radiotherapy, and radiation quality assurance, as well as in industrial and security screening.[2–5] Si, $\alpha$-Se, and Cd(Zn)Te are the most commonly used semiconductors in modern direct X-ray detectors.[4] While these inorganic semiconductors afford X-ray detectors with decent performance, numerous issues and challenges still need to be addressed to make them more affordable and improve their performance. Costly production involving energy-consuming high-temperature processing and a lack of structural flexibility are two major drawbacks of conventional inorganic semiconductors.[1,6–10] To address these issues, researchers have been working on new types of semiconductors that offer low-cost preparation and high flexibility.[11] One approach involves blending high-Z X-ray absorbers, such as inorganic nanoparticles (e.g., $Bi_2O_3$) and metal halide perovskites, with polymers to form large, flexible films. However, this approach has proved ineffective due to the non-uniformity of such blended films, evidenced by cracks and traps, resulting in poor detector performance.[12–16]

To achieve large-size films with excellent uniformity for high-performance X-ray detectors, it is essential to develop material systems that combine high X-ray absorbers, such as metal oxides and halides, with organic materials in singular orientations, free from phase segregation. Zero-dimensional (0D) organic metal halide hybrids (OMHHs), which incorporate high X-ray-absorbing metal halides and semiconducting organic cations through ionic bonding, emerge as highly promising candidates for this purpose. In 2024, we reported efficient direct X-ray detectors based on single crystalline 0D OMHH $(TPA\text{-}P)_2ZnBr_4$ ($TPA\text{-}P^+$ = 4-(4-(diphenylamino)phenyl)-1-propylpyridin-1-ium) with molecular sensitization, in which metal halide species ($ZnBr_4^{2-}$) act as X-ray absorbers and organic semiconducting cations ($TPA\text{-}P^+$) as charge transporters.[17] Molecular sensitization in 0D OMHHs provides unique molecular design and engineering opportunities, creating avenues to rationally select organic species with desired intrinsic properties like electrical

[*] O. J Olasupo, A. M. Adewolu, M. Khizr, T. F. Manny, H. Liu, M. S. Islam, S. Moslemi, J. R. V Winfred, T. N. Gamaralalage, Y.-Y. Hu, R. Das, B. Ma
Department of Chemistry and Biochemistry, Florida State University, Tallahassee, Florida 32306, USA
E-mail: bma@fsu.edu

T. B. Shonde
Department of Chemistry, University of West Florida, Pensacola, Florida 32514, USA

E. Kim
Young Scholars Program, Office of STEM Teaching Activities, Florida State University, Tallahassee, Florida 32306, USA

Additional supporting information can be found online in the Supporting Information section

conductivity and flexibility. However, the scalability of 0D OMHH single crystals is highly limited due to the time-intensive nature of the crystal growth and the challenge of producing large crystals exceeding a few centimeters. We have successfully expanded this class of hybrid materials from solution-grown single crystals to amorphous films by employing non-crystalline organic cations, thereby addressing this limitation.[18] By using (triphenyl(9-phenyl-9H-carbazol-3-yl) phosphonium bromide (TPPCarzBr) to react with $MnBr_2$, large-size amorphous 0D $(TPPCarz)_2MnBr_4$ films can be easily prepared with remarkable scintillation performance and long-term stability. The amorphous feature of 0D $(TPPCarz)_2MnBr_4$ enables exceptional processability, allowing it to be shaped into various forms on demand and re-softened and reshaped multiple times, similar to thermoplastics.[19] These results indicate that direct X-ray detectors utilizing large-scale amorphous 0D OMHH films are feasible with the right combination of organic cations and metal halides, specifically non-crystalline semiconducting organic cations paired with wide-bandgap metal halides to enable molecular sensitization.

Here, we report on the development of solution-processed amorphous 0D OMHH films with molecular sensitization for efficient direct X-ray detection. By reacting non-crystalline organic halide salt, TPPCarzBr, with wide-bandgap metal halide, $ZnBr_2$, we have successfully fabricated large-area, uniform, and amorphous 0D OMHH, $(TPPCarz)_2ZnBr_4$ films for the first time. Similar to single-crystalline 0D $(TPA\text{-}P)_2ZnBr_4$, the amorphous 0D $(TPPCarz)_2ZnBr_4$ exhibits highly efficient molecular sensitization, where $ZnBr_4^{2-}$ anions serve as X-ray absorbers and $TPPCarz^+$ cations function as charge transporters.[17] Direct X-ray detectors based on amorphous 0D $(TPPCarz)_2ZnBr_4$ films have been successfully fabricated and tested. At an electric field of 20 V $mm^{-1}$, these detectors exhibit a high resistivity of $1.82 \times 10^{10}$ Ω cm, an impressive sensitivity of 2165 μC $Gy_{air}{}^{-1}cm^{-2}$, and a very low detection limit of 6.01 $nGy_{air}$ $s^{-1}$, achieving performance comparable to conventional inorganic semiconductor-based devices.[20] Additionally, a large-area detector (~3 cm in diameter) was fabricated using 0D $(TPPCarz)_2ZnBr_4$ films, demonstrating a record high sensitivity of 1802 μC $Gy_{air}{}^{-1}cm^{-2}$ for large-area solution-processed detectors.

## Results and Discussion

Figure 1a shows the molecular sensitization scheme in 0D OMMHs, where metal halides act as X-ray absorbers and organic cations as charge transporters. In this work, we aimed to develop amorphous 0D OMHH films, rather than single crystals, for direct X-ray detectors, as depicted in Figure 1b. TPPCarzBr was chosen as the non-crystalline organic salt due to its semiconducting nature, which has been previously demonstrated to form amorphous 0D OMHH films when reacted with $MnBr_2$ via simple solution processing.[18] Details of TPPCarzBr synthesis can be found in Scheme S1 of the supporting information. By replacing $MnBr_2$ with the wider-bandgap $ZnBr_2$ in the reaction with TPPCarzBr, we obtained 0D $(TPPCarz)_2ZnBr_4$, enabling molecular sensitization of $TPPCarz^+$ cations by $ZnBr_4^{2-}$ anions. The preparation of amorphous 0D $(TPPCarz)_2ZnBr_4$ films is illustrated in Figure 1c. Specifically, a precursor solution was prepared by dissolving TPPCarzBr and $ZnBr_2$ in a 2:1 mole ratio at the desired concentrations in dimethylformamide (DMF) solvent at room temperature. The solution was then cast into a resin mold and heated at approximately 150 °C inside a fume hood for 2 days to remove the solvent (see details in the Experimental Section). The resulting films, exhibiting excellent uniformity and smoothness, could be easily removed from the mold, with their size, thickness, and area readily adjustable by varying the precursor solution concentration, amount, and mold dimensions.

To confirm that the prepared 0D $(TPPCarz)_2ZnBr_4$ films possessed the desired chemical composition and film morphology, we conducted compositional, structural, morphological, and photophysical characterizations. Energy-dispersive X-ray spectroscopy (EDS) analysis, as shown in Figure 2a, reveals the presence of all expected elements, namely, C, N, P, Zn, and Br, with a uniform spatial distribution throughout the film. The successful formation of 0D $(TPPCarz)_2ZnBr_4$ through this simple solution processing, followed by mild thermal annealing, was further verified by the close agreement between the measured elemental composition and the theoretical weight percentages, corresponding to the 2:1 mole ratio of TPPCarzBr and $ZnBr_2$, as presented in both Figure S1 and Table S1. Likewise, to confirm the presence of zinc bromide bonds in 0D $(TPPCarz)_2ZnBr_4$, we recorded the Raman spectra as shown in Figure S2, where Zn-Br stretching vibration could be seen at ~190 $cm^{-1}$.[21] We used a scanning electron microscope (SEM) to evaluate the film's surface smoothness. As shown in Figure 2b, the SEM image exhibits a featureless surface, indicating excellent uniformity and smoothness, which are critical for detector applications.

The amorphous feature of the solution-processed films was confirmed by using powder X-ray diffraction (PXRD). As shown in Figure 2c, the PXRD pattern displays distinct broad diffraction features ranging from $2\theta = 5$ to 50°, in contrast to the sharp diffracting peaks observed in crystalline 0D OMHHs, providing clear evidence of the film's intrinsic amorphous nature.[17,22,23] With the compositional and structural properties of 0D $(TPPCarz)_2ZnBr_4$ films characterized, we investigated the basic photophysical properties using steady-state optical spectroscopy. Figure 2d shows the photoluminescence (PL) emission spectra of solution-processed TPPCarzBr and 0D $(TPPCarz)_2ZnBr_4$ films, both measured under 365 nm excitation. The deep blue emission of 0D $(TPPCarz)_2ZnBr_4$ films, peaking at ~ 405 nm, closely matches that of TPPCarzBr, indicating that the emission primarily originates from the lower bandgap $TPPCarz^+$ cations, with minimal contribution from the wider bandgap $ZnBr_42^-$ species. Furthermore, time-resolved photoluminescence (TRPL) spectra were recorded for both samples, as shown in Figure S3. The short average decay lifetimes of 1.3 and 2.2 ns, respectively, suggest a common emission origin from $TPPCarz^+$. These results, in contrast to the green emission of 0D $(TPPCarz)_2MnBr_4$ originating from $MnBr_4^{2-}$ species with a lower bandgap than $TPPCarz^+$ cations, validate our material design strategy. Specifically, they

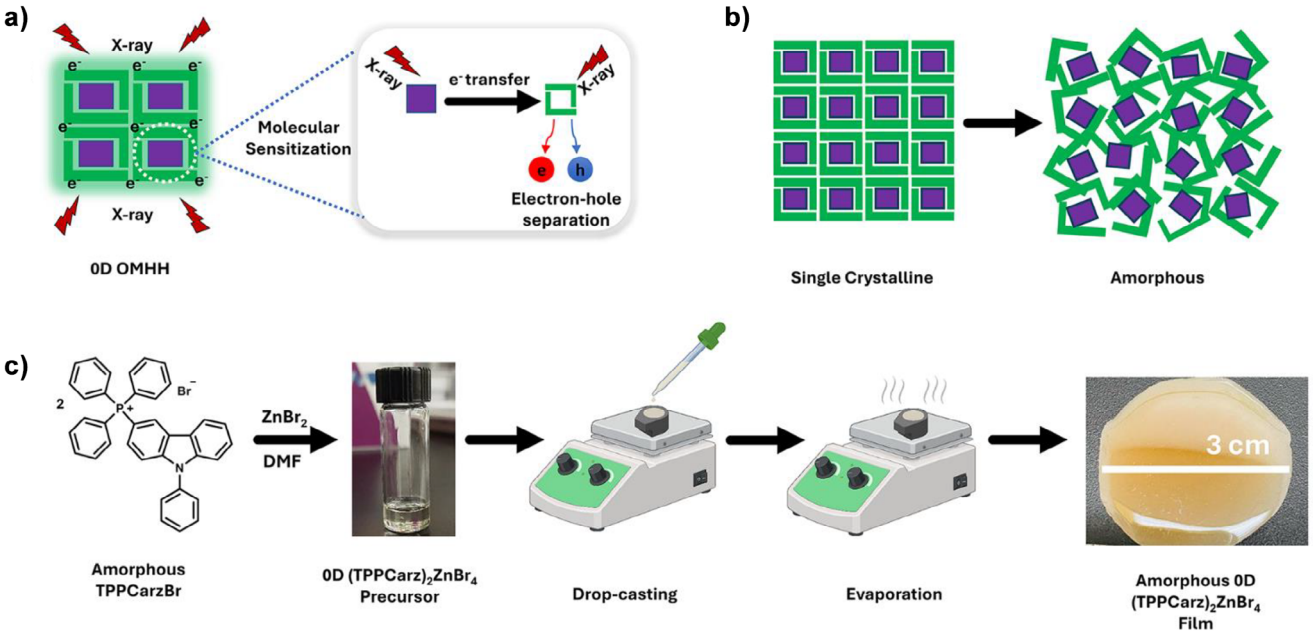


***Figure 1.*** a) Schematic representation of molecular sensitization in 0D OMHHs, where metal halides (purple squares) act as X-ray absorbers and organic cations (green L-shaped blocks) with a lower bandgap as charge transporters. b) From single-crystalline 0D OMHHs to amorphous 0D OMHHs. c) Scheme showing the preparation of amorphous 0D $(TPPCarz)_2ZnBr_4$ films via facile solution processing and thermal annealing.

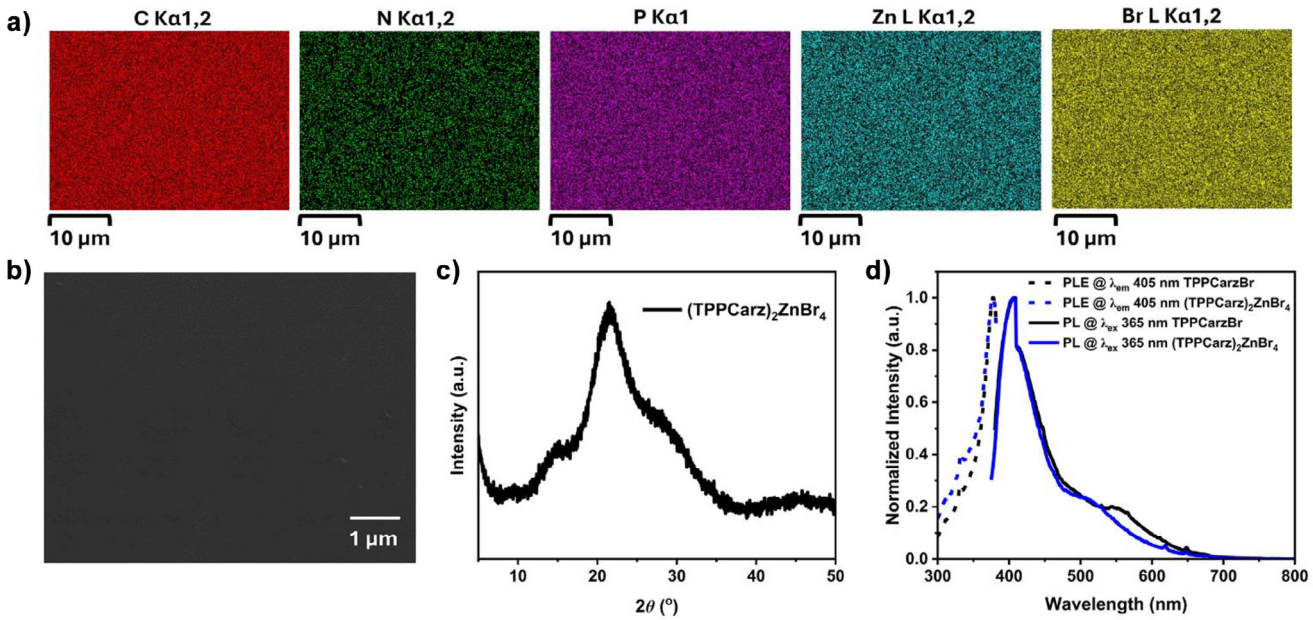


***Figure 2.*** a) Elemental mapping showing the presence of C, N, P, Zn, Br, and their uniform distribution in a solution-processed 0D $(TPPCarz)_2ZnBr_4$ film. b) Scanning electron microscopy (SEM) image of a solution-processed 0D $(TPPCarz)_2ZnBr_4$ film. c) PXRD pattern of a solution-processed 0D $(TPPCarz)_2ZnBr_4$ film. d) Photoluminescence excitation (PLE) (emission at 405 nm) and photoluminescence (PL) emission (excited at 365 nm) spectra of solution-processed TPPCarzBr and 0D $(TPPCarz)_2ZnBr_4$ films.

demonstrate the successful integration of wide-bandgap metal halide anions with smaller-bandgap organic cations, a key requirement for achieving efficient molecular sensitization of organic cations by metal halides.[24]

The optical bandgap of amorphous 0D $(TPPCarz)_2ZnBr_4$ films was estimated from the ultraviolet-visible absorption spectrum, as shown in Figure 3a. With an absorption edge at ~ 402 nm, 0D $(TPPCarz)_2ZnBr_4$ has an optical bandgap of around 3.0 eV, as determined by Tauc plot analysis (inset of Figure 3a), placing it within the semiconductor range. To characterize the electronic properties of amorphous 0D $(TPPCarz)_2ZnBr_4$ films, we fabricated a simple two-terminal vertical device (inset of Figure 3b) using a 1 mm-thick 0D $(TPPCarz)_2ZnBr_4$ film. The dark bulk resistivity measured as

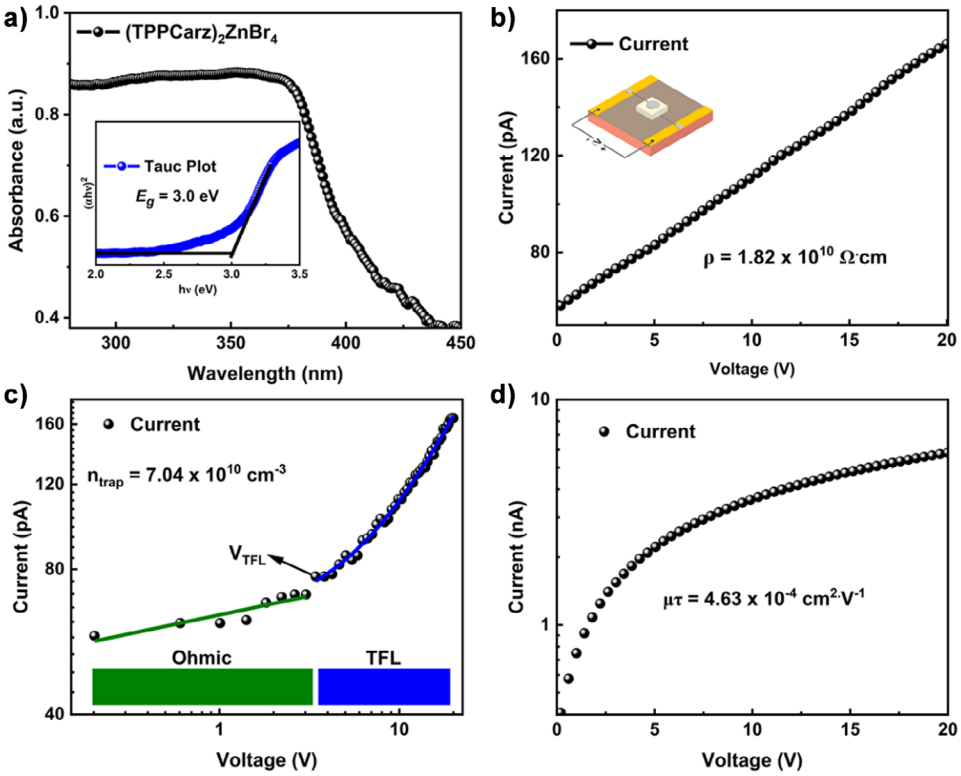


***Figure 3.*** a) UV–vis solid-state absorptance spectrum of solution-processed 0D $(TPPCarz)_2ZnBr_4$ films, with the inset showing an estimated bandgap of 3.0 eV. b) Current-voltage (I-V) plot showing the dark resistivity of a 1-mm-thick film in a vertical device structure. The inset shows the schematic of the device structure. c) Dark I-V of a 0D $(TPPCarz)_2ZnBr_4$ film fitted under the space charge-limited current (SCLC) model. d) Bias-dependent photoconductivity of a 0D $(TPPCarz)_2ZnBr_4$-based detector under continuous X-ray irradiation of 221.39 $\mu Gy_{air} s^{-1}$.

$\sim 1.82 \times 10^{10}$ Ω cm is comparable to that of molten-grown CdZnTe ($3 \times 10^{10}$ Ω cm)[7,20] and previously reported 0D lead-free metal halide single crystals ($\sim 10^{10}$ Ω cm),[22,23] but significantly higher than most of the metal halide perovskite single crystals ($\sim 10^{7-}$ $10^{9}$ Ω cm).[7,25] Similar to 0D $(TPA-P)_2ZnBr_4$ single crystals, the high dark resistivity recorded here in 0D $(TPPCarz)_2ZnBr_4$ films is attributed to the 0D structure, which has low intrinsic carrier concentrations that effectively suppress dark current and eliminate unfavorable baseline drifting of detectors under real-life operation.[25] Fitting the dark current-voltage (I-V) curve with the space charge-limited current (SCLC) model (Figure 3c) revealed two distinct regimes, corresponding to $I \propto V^n$: Ohmic ($n = 1$) and Trap-Filling Limited (TFL, $n > 2$) regimes. The density of trap states, $n_{trap}$ of 0D $(TPPCarz)_2ZnBr_4$ was calculated using Equation (1) below:

$$n_{trap} = \frac{2V_{TFL}\varepsilon\varepsilon_0}{eL^2} \quad (1)$$

Where $V_{TFL} = 3.46$ V represents the onset trap-filling voltage (the voltage corresponding to the regime where all the available trap states are filled with injected carriers from the metal electrodes), $\varepsilon$ is the permittivity estimated from the Capacitance versus Frequency plot (shown in Figure S4), $\varepsilon_0$ = the vacuum permittivity ($8.854 \times 10^{-12}$ F·m$^{-1}$), $e$ = elementary charge ($1.602 \times 10^{-19}$ C), and $L$ = the thickness of the film sample (1 mm). Using these parameters, we determined the $n_{trap}$ value of solution-processed amorphous 0D $(TPPCarz)_2ZnBr_4$ films to be $7.04 \times 10^{10}$ cm$^{-3}$, a remarkably low value.

This suggests the film's defect-free nature, which is highly advantageous for minimizing charge carrier recombination and enhancing carrier extraction efficiency.[25,26] Indeed, this trap density is significantly lower than that of many commercially available inorganic semiconductors, including polycrystalline Si ($10^{13}$–$10^{14}$ cm$^{-3}$) and CdTe/CdS ($10^{11}$–$10^{13}$ cm$^{-3}$), as well as pure crystalline organic semiconductors like pentacene ($10^{14}$–$10^{15}$ cm$^{-3}$) and rubrene ($\sim 10^{16}$ cm$^{-3}$).[27–31] To evaluate the charge carrier collection efficiency of 0D $(TPPCarz)_2ZnBr_4$ films for direct X-ray detection, we measured the charge carrier mobility lifetime product ($\mu\tau$)under a continuous X-ray irradiation of 221.39 $\mu Gy_{air}$ s$^{-1}$. As shown in Figure 3d, the voltage-dependent photoconductivity $\mu\tau$ was estimated to be $4.63 \times 10^{-4}$ cm$^2$V$^{-1}$ using the Modified Hecht equation (Equation (2) below):[32]

$$I = \frac{I_0\mu\tau V}{L^2}\left[1 - exp\left(\frac{-L^2}{\mu\tau V}\right)\right] \quad (2)$$

where $L$ is the thickness of the 0D $(TPPCarz)_2ZnBr_4$ film sample (1 mm) sandwiched between two vertical silver electrodes with a $1 \times 1$ mm$^2$ area, and $I_0$ represents the saturated photocurrent reached under a 20 V

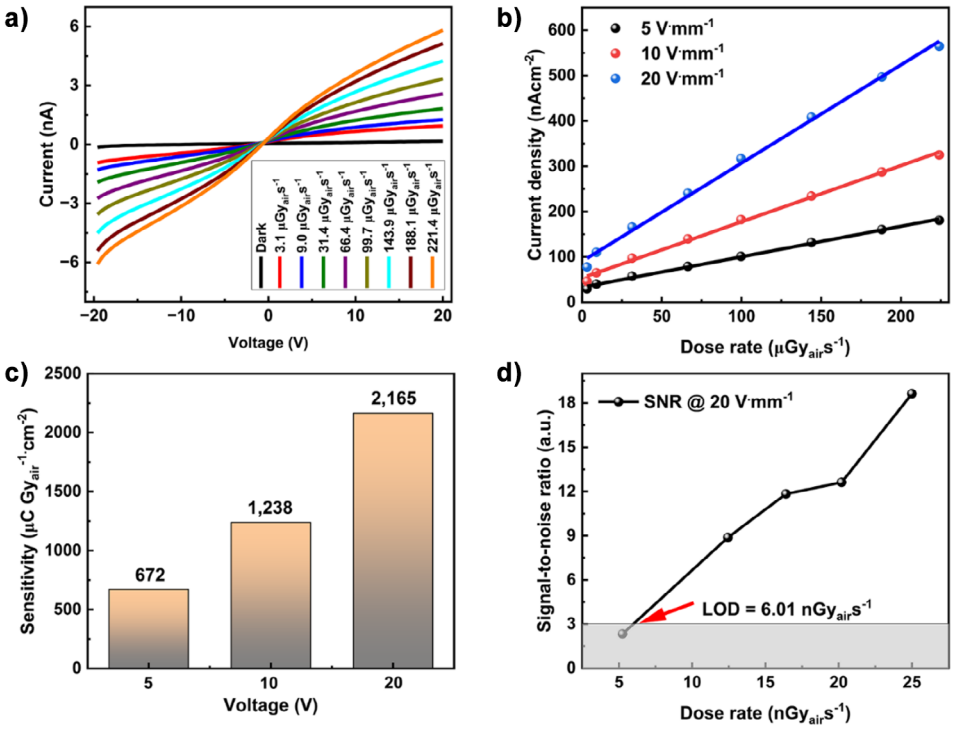


***Figure 4.*** a) X-ray detection I-V plot at 20 V mm$^{-1}$ electric field from dark to an X-ray dose rate of 221.39 μGy$_{air}$s$^{-1}$. b) X-ray photocurrent density at various electric fields. c) Calculated X-ray sensitivity at different voltages/electric fields. d) The signal-to-noise ratio (SNR) of 0D $(TPPCarz)_2ZnBr_4$ detectors versus various dose rates. The detection limit (LOD) of 6.01 nGy$_{air}$s$^{-1}$, estimated at 20 V mm$^{-1}$, corresponds to the signal at an SNR of ~3.

bias voltage. The high-mobility lifetime product of 0D $(TPPCarz)_2ZnBr_4$ films can be attributed to the presence of the charge-conducting organic cations, $TPPCarz^+$. This value is comparable to that of commercially available inorganic CdZnTe (~$10^{-3}$–$10^{-5}$ cm$^2$V$^{-1}$)[10,20,33] and $CsPbBr_3$ detectors (~$10^{-3}$ cm$^2$V$^{-1}$),[34,35] and much higher than that of $\alpha$-Se detectors ($10^{-7}$ cm$^2$V$^{-1}$).[36–39]

The outstanding electrical properties of solution-processed amorphous 0D $(TPPCarz)_2ZnBr_4$ films, including high bulk resistivity, low density of trap states, and a large $\mu\tau$, make them highly promising semiconductors for direct X-ray detectors.[6] To further evaluate its capabilities, we fabricated direct X-ray detectors based on 0D $(TPPCarz)_2ZnBr_4$ films and tested their performance at various electric fields and X-ray doses inside a homemade dark box. A tungsten anode X-ray tube with a maximum voltage of 40 kV and a current of 100 μA was used as the radiation source. Under an applied electric field of 20 V mm$^{-1}$ in ambient air, we investigated the effect of increasing the X-ray dose rate on the measured photocurrent. As shown in Figure 4a, the I-V plot reveals a significant photocurrent increase at 20 V mm$^{-1}$ when transitioning from dark conditions to an X-ray dose of 3.1 μGy$_{air}$s$^{-1}$. Results for similar I-V measurements at 5 V mm$^{-1}$ and 10 V mm$^{-1}$ are provided in Figures S5a and S5b, respectively. Moreover, Figure 4a demonstrates that 0D $(TPPCarz)_2ZnBr_4$ detectors exhibited exceptional operational stability, with a consistent increase in photocurrent as the X-ray tube current was adjusted from 20 to 100 μA, reaching a maximum X-ray dose of 221.39 μGy$_{air}$s$^{-1}$. Like in X-ray detectors based on 0D $(TPA\text{-}P)_2ZnBr_4$ single crystals,[17] a well-suppressed ionic migration is achieved in devices based on amorphous 0D $(TPPCarz)_2ZnBr_4$ films. This is attributed to their 0D structure, where the bulky $TPPCarz^+$ cations introduce steric effects that increase the activation energy barrier for ionic migration.

The sensitivity and limit of detection are two other critical performance metrics of X-ray detectors, particularly in medical applications.[25] We measured the photocurrent under varying electric fields and increasing X-ray dose rates to determine the sensitivity of amorphous 0D $(TPPCarz)_2ZnBr_4$ film-based detectors. As expected for an ideal X-ray detector, Figure 4b displays a perfectly linear relationship between the generated photocurrent densities and the X-ray dose rates across all tested electric fields. The sensitivity ($S$) was extracted from the plots of current density ($J_{X-ray}$ and $J_{dark}$ represent photocurrent and dark current densities) versus X-ray dose rate ($D$) at different voltages using Equation (3) below:

$$S = \frac{(J_{X-ray} - J_{dark})}{D} \tag{3}$$

As shown in Figure 4c, the sensitivity of amorphous 0D $(TPPCarz)_2ZnBr_4$ film-based detectors was measured at different electric fields, yielding 672 μC Gy$_{air}$$^{-1}$cm$^{-2}$ at 5 V mm$^{-1}$ and increasing to 1238 μC Gy$_{air}$$^{-1}$cm$^{-2}$ at 10 V mm$^{-1}$. Notably, a high sensitivity of 2165 μC Gy$_{air}$$^{-1}$cm$^{-2}$ was recorded at 20 V mm$^{-1}$, significantly outperforming commercially amorphous $\alpha$-Se-based detectors (440 μC Gy$_{air}$$^{-1}$cm$^{-2}$),

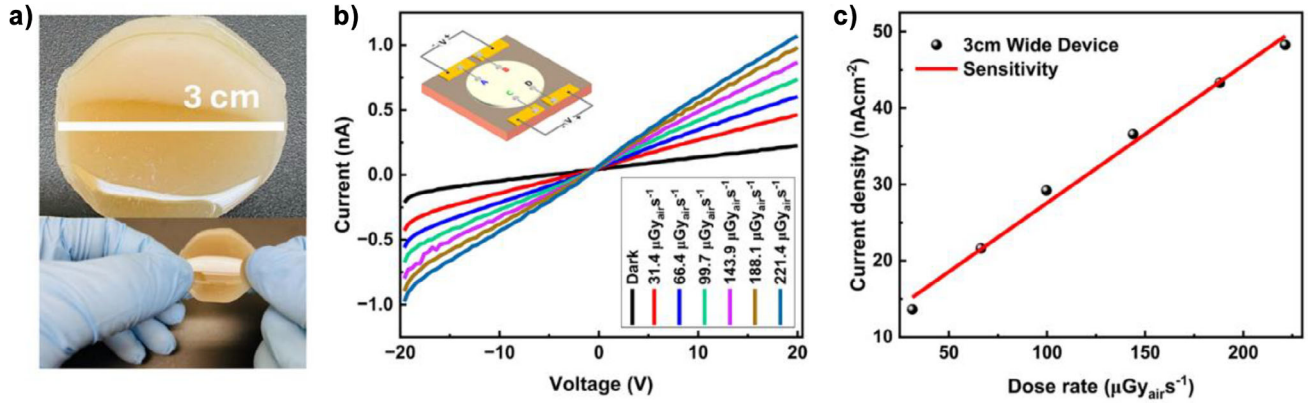


***Figure 5.*** a) Images of a 3 cm wide solution processed 0D $(TPPCarz)_2ZnBr_4$ film. b) X-ray detection I-V plot of a device based on 3 cm wide 0D $(TPPCarz)_2ZnBr_4$ film at 20 V $mm^{-1}$ electric field from dark to an X-ray dose rate of 221.39 $\mu Gy_{air}s^{-1}$ (inset shows the lateral device structure). c) X-ray photocurrent density versus dose rate with an estimated sensitivity of 1802 $\mu C\ Gy_{air}^{-1}cm^{-2}$.

which require a much higher operating electric field of 15, 000 V $mm^{-1}$.[40]

Our amorphous 0D $(TPPCarz)_2ZnBr_4$ film-based detectors operated at a field of 20 V $mm^{-1}$ also exhibit better performance than several reported lead-free bismuth-based materials, including 3D $Cs_2AgBiBr_6$ single crystals (1974 $\mu C\ Gy_{air}^{-1}cm^{-2}$ at 50 V $mm^{-1}$),[41] 0D $(R\text{-}PPA)_2BiI_5$ single crystals (150 $\mu C\ Gy_{air}^{-1}cm^{-2}$ at 10 $Vmm^{-1}$),[23] 0D $MA_3Bi_2I_9$ single crystals (1947 $\mu C\ Gy_{air}^{-1}cm^{-2}$ at 60 V $mm^{-1}$),[22] and comparable to the recently reported 0D $AG_3Bi_2I_9$ polycrystalline wafers (2675 $\mu C\ Gy_{air}^{-1}cm^{-2}$ at 20 $Vmm^{-1}$).[42] The X-ray detection limit (LOD) of amorphous 0D $(TPPCarz)_2ZnBr_4$ film-based detectors at 20 V $mm^{-1}$ was determined to be 6.01 $nGy_{air}s^{-1}$, as shown in Figure 4d, where LOD is the equivalent X-ray dose rate corresponding to a signal-to-noise ratio (SNR) of 3. This exceptionally low LOD is the best reported to date for 0D OMHHs-based X-ray detectors.[22,23,42] Notably, this LOD value is more than 900 times lower than the X-ray dose rate of 5.5 $\mu Gy_{air}s^{-1}$ required for standard medical diagnostics, highlighting the immense potential of our amorphous 0D $(TPPCarz)_2ZnBr_4$ films for safe and high-performance X-ray detectors in medical applications.[43,44] Table S2 summarizes the performance of devices based on our amorphous 0D $(TPPCarz)_2ZnBr_4$ films in comparison with existing amorphous materials, including $\alpha$-Se and other organic–inorganic hybrid films.

To further demonstrate the feasibility of fabricating large-area X-ray detectors using solution-processed amorphous 0D $(TPPCarz)_2ZnBr_4$ films, we prepared a larger film that is about 30 times larger than the 1 x 1 mm film, and approximately 3 cm in diameter (Figure 5a) with a thickness of ~1 mm (Figure S6a) using a larger mold. X-ray detectors were then fabricated using a lateral device architecture with silver electrodes (Figures S6b and S6c). We evaluated the performance of large-area detectors under similar test conditions as before, applying an electric field of 20 V $mm^{-1}$ and X-ray dose rates up to 221.39 $\mu Gy_{air}s^{-1}$. As shown in the I-V plot in Figure 5b, the detector exhibited stable performance and a steady increase in the measured photocurrent across the entire range of X-ray dose rates applied. Remarkably, the 3 cm wide detector achieved an impressive sensitivity of 1802 $\mu C\ Gy_{air}^{-1}cm^{-2}$ at 20 $Vmm^{-1}$ (Figure 5c), which suggests that the 0D $(TPPCarz)_2ZnBr_4$ film is a potential candidate for larger area detector applications.

## Conclusion

In summary, we have successfully developed high-quality, large-area amorphous 0D $(TPPCarz)_2ZnBr_4$ films using a facile solution-processing technique for the first time. These films exhibited exceptional electronic properties, including a large bulk resistivity of $1.82 \times 10^{10}$ Ω cm, a high $\mu\tau$ of $4.63 \times 10^{-4}$ $cm^2V^{-1}$, an impressive sensitivity of 2165 $\mu C\ Gy_{air}^{-1}cm^{-2}$, and an ultra-low detection limit of 6.01 $nGy_{air}s^{-1}$, representing the best performance reported to date for solution-processed amorphous materials-based X-ray detectors. Moreover, 0D $(TPPCarz)_2ZnBr_4$ films can be readily processed into large-area (~3 cm diameter) flat detector films and seamlessly integrated with external readout circuitry for high-performance X-ray detection in ambient air. Our work highlights the exceptional tunability of 0D OMHHs, particularly their facile solution processability, versatility, and unique material properties, making them promising candidates for next-generation large-area flat panel detectors.

## Supporting Information

The authors have cited additional references within the Supporting Information.[45–48]

## Acknowledgements

The authors acknowledge support from the National Science Foundation (DMR-2204466) and the Florida State University Office of Research. Part of this work utilized resources provided by the Materials Characterization Laboratory (FSU075000MAC) at the FSU Department of Chemistry

and Biochemistry. E.K. thanks the support from the Young Scholars Program at FSU.

## Conflict of Interests

A provisional patent application entitled "Direct X-ray Detectors Based on Solution-Processed Amorphous Zero-Dimensional Organic Metal Halide Hybrid Films" (application number 63/783528) has been filed with the United States Patent and Trademark Office on April 4, 2025. O. J. O. and B. M. are listed as inventors.

## Data Availability Statement

The data that support the findings of this study are available in the Supporting Information of this article.

**Keywords:** Large-area devices · Semiconductors · Solution-processed amorphous films · X-ray detectors · Zero-dimensional organic metal halide hybrids

[1] S. O. Kasap, J. A. Rowlands, *Proc. IEEE* **2002**, *90*, 591–604.
[2] Y. He, J. Song, M. Li, K. Sakhatskyi, W. Li, X. Feng, B. Yang, M. Kovalenko, H. Wei, *Nat. Photonics* **2024**, *18*, 1052–1058.
[3] C. Woodford, P. Ashby, in *The Fourth Conf. on Nucl. Sci. Eng. in Australia 2001, Conf. Handbook, Australia*, Australian Nuclear Association Inc., Sutherland, New South Wales, *198*, pp. 98–100.
[4] M. Yaffe, J. Rowlands, *Physics in Medicine & Biology* **1997**, *42*, 1.
[5] S. Pettinato, M. Girolami, R. Olivieri, A. Stravato, C. Caruso, S. Salvatori, *Materials* **2021**, *14*, 5203.
[6] H. Wei, J. Huang, *Nat. Commun.* **2019**, *10*, 1066.
[7] X. Ou, F. Gao, *Nat. Commun.* **2024**, *15*, 5754.
[8] S. Yakunin, M. Sytnyk, D. Kriegner, S. Shrestha, M. Richter, G. J. Matt, H. Azimi, C. J. Brabec, J. Stangl, M. V. Kovalenko, *Nat. Photonics* **2015**, *9*, 444–449.
[9] S. Kasap, J. B. Frey, G. Belev, O. Tousignant, H. Mani, J. Greenspan, L. Laperriere, O. Bubon, A. Reznik, G. DeCrescenzo, *Sensors* **2011**, *11*, 5112–5157.
[10] K. Iniewski, *J. Instrum.* **2014**, *9*, C11001.
[11] S. Lai, P. Cosseddu, L. Basiricò, A. Ciavatti, B. Fraboni, A. Bonfiglio, *Adv. Electron. Mater.* **2017**, *3*, 1600409.
[12] H. Thirimanne, K. Jayawardena, A. Parnell, R. Bandara, A. Karalasingam, S. Pani, J. Huerdler, D. Lidzey, S. Tedde, A. Nisbet, *Nat. Commun.* **2018**, *9*, 2926.
[13] L. Mao, Y. Li, H. Chen, L. Yu, J. Zhang, *Nanomaterials* **2021**, *11*, 1832.
[14] H. Li, X. Shan, J. N. Neu, T. Geske, M. Davis, P. Mao, K. Xiao, T. Siegrist, Z. Yu, *J. M. Chem. C* **2018**, *6*, 11961–11967.
[15] X. Liu, H. Li, Q. Cui, S. Wang, C. Ma, N. Li, N. Bu, T. Yang, X. Song, Y. Liu, *Angew. Chem.* **2022**, *134*, e202209320.
[16] C. Liang, S. Zhang, L. Cheng, J. Xie, F. Zhai, Y. He, Y. Wang, Z. Chai, S. Wang, *Angew. Chem. Int. Ed.* **2020**, *59*, 11856–11860.
[17] O. J. Olasupo, T.-H. Le, T. B. Shonde, H. Liu, A. Bouchard, S. Bouchard, T. N. Gamaralalage, A. M. Adewolu, T. F. Manny, X. Lin, *ACS Energy Lett.* **2024**, *9*, 5704–5711.
[18] T. F. Manny, T. B. Shonde, H. Liu, M. S. Islam, O. J. Olasupo, J. Viera, S. Moslemi, M. Khizr, C. Chung, J. R. V. Winfred, *Adv. Funct. Mater.* **2024**, 2413755.
[19] T. Yeşil, A. Mutlu, S. Siyahjani Gültekin, Z. G. l. Günel, C. Zafer, *ACS Omega* **2023**, *8*, 27784–27793.
[20] A. Owens, *J. Synchrotron Radiat.* **2006**, *13*, 143–150.
[21] S. Yannopoulos, A. Kalampounias, A. Chrissanthopoulos, G. Papatheodorou, *J. Chem. Phys.* **2003**, *118*, 3197–3214.
[22] Y. Liu, Z. Xu, Z. Yang, Y. Zhang, J. Cui, Y. He, H. Ye, K. Zhao, H. Sun, R. Lu, *Matter* **2020**, *3*, 180–196.
[23] S. You, Z. K. Zhu, S. Dai, J. Wu, Q. Guan, T. Zhu, P. Yu, C. Chen, Q. Chen, J. Luo, *Adv. Funct. Mater.* **2023**, *33*, 2303523.
[24] T. B. Shonde, M. Chaaban, H. Liu, O. J. Olasupo, A. Ben-Akacha, F. G. Gonzalez, K. Julevich, X. Lin, J. R. V. Winfred, L. M. Stand, *Adv. Mater.* **2023**, *35*, 2301612.
[25] X. Xu, W. Qian, S. Xiao, J. Wang, S. Zheng, S. Yang, *EcoMat* **2020**, *2*, e12064.
[26] D. Shi, V. Adinolfi, R. Comin, M. Yuan, E. Alarousu, A. Buin, Y. Chen, S. Hoogland, A. Rothenberger, K. Katsiev, *Science* **2015**, *347*, 519–522.
[27] J. R. Ayres, *J. Appl. Phys.* **1993**, *74*, 1787–1792.
[28] I. Capan, V. Borjanović, B. Pivac, *Sol. Energy Mater. Sol. Cells* **2007**, *91*, 931–937.
[29] A. Balcioglu, R. Ahrenkiel, F. Hasoon, *J. Appl. Phys.* **2000**, *88*, 7175–7178.
[30] C. Goldmann, C. Krellner, K. P. Pernstich, S. Haas, D. J. Gundlach, B. Batlogg, *J. Appl. Phys.* **2006**, *99*, 034507.
[31] Y. S. Yang, S. H. Kim, J.-I. Lee, H. Y. Chu, L.-M. Do, H. Lee, J. Oh, T. Zyung, M. K. Ryu, M. S. Jang, *Appl. Phys. Lett.* **2002**, *80*, 1595–1597.
[32] Y. Feng, L. Pan, H. Wei, Y. Liu, Z. Ni, J. Zhao, P. N. Rudd, L. R. Cao, J. Huang, *J. Mater. Chem.* **2020**, *8*, 11360–11368.
[33] M. D. Alam, S. S. Nasim, S. Hasan, *Prog. Nucl. Energy* **2021**, *140*, 103918.
[34] Y. He, I. Hadar, M. G. Kanatzidis, *Nat. Photonics* **2022**, *16*, 14–26.
[35] J. Pang, H. Wu, H. Li, T. Jin, J. Tang, G. Niu, *Nat. Commun.* **2024**, *15*, 1769.
[36] J. Stavro, A. H. Goldan, W. Zhao, *Eur. J. Radiol.* **2018**, *5*, 043502–043502.
[37] S. Kasap, *J. Phys. D: Appl. Phys.* **2000**, *33*, 2853–2865.
[38] M. Kabir, S. M. Arnab, N. Hijazi, *J. Mater. Sci.:Mater. Electron.* **2019**, *30*, 21059–21063.
[39] H. Huang, S. Abbaszadeh, *IEEE Sens. J.* **2019**, *20*, 1694–1704.
[40] M. Choquette, H. Rougeot, J.-P. Martin, L. Laperriere, Z. Shukri, B. T. Polischuk, in *Medical Imaging 2000: Physics of Medical Imaging, Vol. 3977*, SPIE, Bellingham, Washington, USA, **2000**, pp. 128–136.
[41] L. Yin, H. Wu, W. Pan, B. Yang, P. Li, J. Luo, G. Niu, J. Tang, *Adv. Opt. Mater.* **2019**, *7*, 1900491.
[42] J. Yu, Y. Luo, N. Tian, Y. Liu, Z. Yang, J. Pi, L. Li, R. Zheng, C. Wang, S. Liu, *Adv. Mater.* **2024**, 2413709.
[43] I. Clairand, J.-M. Bordy, E. Carinou, J. Daures, J. Debroas, M. Denozière, L. Donadille, M. Ginjaume, C. Itié, C. Koukorava, *Radiat. Meas.* **2011**, *46*, 1252–1257.
[44] D. R. Shearer, M. Bopaiah, *Health Phys.* **2000**, *79*, S20–S21.
[45] L.-J. Xu, M. Worku, Q. He, H. Lin, C. Zhou, B. Chen, X. Lin, Y. Xin, B. Ma, *J. Phys. Chem. Lett.* **2019**, *10*, 5836–5840.
[46] H. Liu, T. B. Shonde, F. Gonzalez, O. J. Olasupo, S. Lee, D. Luong, X. Lin, J. R. Vellore Winfred, E. Lochner, I. Fatima, *Adv. Mater.* **2023**, *35*, 2209417.
[47] H. Liang, S. Cui, R. Su, P. Guan, Y. He, L. Yang, L. Chen, Y. Zhang, Z. Mei, X. Du, *ACS Photonics* **2019**, *6*, 351–359.
[48] Y. Xu, Z. Li, C. Shi, Y. Li, Y. Lei, G. Peng, T. Yu, H. Ren, H. Wang, H. Fan, *Adv. Mater.* **2024**, *36*, 2406128.

Manuscript received: April 30, 2025
Revised manuscript received: June 25, 2025
Accepted manuscript online: June 27, 2025
Version of record online: ■■, ■■

# Research Article

**Direct X-ray Detectors**

O. J Olasupo, A. M. Adewolu, M. Khizr, T. F. Manny, H. Liu, T. B. Shonde, M. S. Islam, S. Moslemi, E. Kim, J. R. V Winfred, T. N. Gamaralalage, Y.-Y. Hu, R. Das, B. Ma* —— **e202509589**

Solution-Processed Amorphous Zero-Dimensional Organic Metal Halide Hybrid Films for Direct X-Ray Detectors

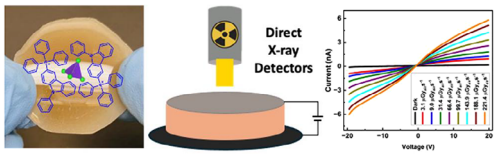


The use of solution-processed amorphous zero-dimensional organic metal halide hybrid $(TPPCarz)_2ZnBr_4$ films for direct X-ray detection is demonstrated. The amorphous films exhibit efficient molecular sensitization, with $ZnBr_4^{2-}$ species serving as X-ray absorbers and $TPPCarz^+$ moieties as charge transporters. The resulting detectors achieve a detection sensitivity of 2165 μC $Gy_{air}^{-1}cm^{-2}$ at 20 V $mm^{-1}$ and a detection limit of 6.01 $nGy_{air}$ $s^{-1}$.